Nanoscale Advances

ROYAL SOCIETY OF CHEMISTRY

PAPER

View Article Online
View Journal | View Issue

Check for updates

Cite this: *Nanoscale Adv.*, 2023, **5**, 6714

A 5-aminoisophthalic acid low molecular weight gelator based novel semiconducting supramolecular Zn(II)-metallogel: unlocking an efficient Schottky barrier diode for microelectronics†

Subhendu Dhibar,*[a] Baishakhi Pal,[b] Kripasindhu Karmakar,[a] Sanjay Roy,[c] Sk Abdul Hafiz,[d] Arpita Roy,[e] Subham Bhattacharjee,[d] Soumya Jyoti Ray,[e] Partha Pratim Ray *[b] and Bidyut Saha *[a]

A novel method has been successfully developed for creating supramolecular metallogels using zinc(II) ions and 5-aminoisophthalic acid as the gelator (low molecular weight gelator) in a dimethylformamide (DMF) solvent at room temperature. Comprehensive rheological investigations confirm the robust mechanical strength of the resulting zinc(II)-metallogel. Microstructural analysis conducted through field-emission scanning electron microscopy (FESEM) unveils a unique flake-like morphology, with energy-dispersive X-ray (EDX) elemental mapping confirming the prevalence of zinc as the primary constituent of the metallogel. To understand the formation mechanism of this metallogel, Fourier-transform infrared (FT-IR) spectroscopy was employed. Notably, these supramolecular zinc(II)-metallogel assemblies exhibit electrical conductivity reminiscent of metal–semiconductor (MS) junction electronic components. Surprisingly, the metallogel-based thin film device showcases an impressive electrical conductivity of 1.34×10^{-5} S m^{-1}. The semiconductor characteristics of the synthesized zinc(II)-metallogel devices, including their Schottky barrier diode properties, have been extensively investigated. This multifaceted study opens up a promising avenue for designing functional materials tailored for electronic applications. It harnesses the synergistic properties of supramolecular metallogels and highlights their significant potential in the development of semiconductor devices. This work represents a novel approach to the creation of advanced materials with unique electronic properties, offering exciting prospects for future innovations in electronic and semiconductor technologies.

Received 22nd August 2023
Accepted 13th October 2023

DOI: 10.1039/d3na00671a

rsc.li/nanoscale-advances

Open Access Article. Published on 26 October 2023. Downloaded on 2/20/2026 1:25:55 PM. This article is licensed under a Creative Commons Attribution-NonCommercial 3.0 Unported Licence.

1. Introduction

Gels are a three-dimensional network of molecules held together by cross-linkages, creating a semi-solid, viscous material.[1] They exist in a colloidal state, with gelators forming the dispersed phase and solvent forming the continuous medium. The characteristic soft and elastic behavior of gels can often be confirmed through tests such as the inverted vial method.[2,3] Supramolecular gels offer distinct advantages due to their composition of low molecular weight gelators, diverging from traditional long-chain polymers. Research in this field aims to understand the intricate structures present in gels across different length scales and explore their potential applications in cutting-edge technologies. Gels find wide-ranging uses in the biomedical, pharmaceutical, oil recovery, food, cosmetic, environmental, and conducting device industries, among others.[4–6] Within the 3D soft gel framework, the core constituents constituting the supramolecular gel are gelators and solvent molecules, both held in immobilized states by the gelator molecules themselves.

Gelators derived from polymers such as polyester, poly(ethylene glycol), polyolefins, polycaprolactones, and polycarbonates are frequently utilized to create a diverse range of stable gel compositions.[7] However, low molecular weight gelators (LMWGs) are pivotal components in the realm of supramolecular gel synthesis. Unlike traditional polymeric materials, LMWGs are characterized by their relatively small molecular

[a]Colloid Chemistry Laboratory, Department of Chemistry, The University of Burdwan, Golapbag, Burdwan 713104, West Bengal, India. E-mail: sdhibar@scholar.buruniv.ac.in; bsaha@chem.buruniv.ac.in; Tel: +91 7001575909; +91 9476341691

[b]Department of Physics, Jadavpur University, Jadavpur, Kolkata 700032, India. E-mail: parthap.ray@jadavpuruniversity.in; Tel: +91 3324572844

[c]Department of Chemistry, School of Sciences, Kalyani Regional Centre, Netaji Subhas Open University, West Bengal, India

[d]Department of Chemistry, KaziNazrul University, Asansol 713303, West Bengal, India

[e]Department of Physics, Indian Institute of Technology Patna, Bihar 801106, India

† Electronic supplementary information (ESI) available. See DOI: https://doi.org/10.1039/d3na00671a

© 2023 The Author(s). Published by the Royal Society of Chemistry

Open Access Article. Published on 26 October 2023. Downloaded on 2/20/2026 1:25:55 PM. This article is licensed under a Creative Commons Attribution-NonCommercial 3.0 Unported Licence.

size, which enables them to self-assemble into well-defined structures through non-covalent interactions. These interactions, such as hydrogen bonding, π–π stacking, and van der Waals forces, lead to the formation of organized networks that entrap solvents and create a gel-like structure.[1,8,9] The design and selection of appropriate LMWGs are crucial as they govern the overall gel properties, including mechanical strength, stability, and responsiveness. LMWGs offer remarkable versatility, allowing researchers to fine-tune the gel's properties by adjusting molecular structures and functional groups. Their ability to create supramolecular gels with tailored characteristics has led to significant advancements in various fields, from materials science to drug delivery, offering novel avenues for developing functional and responsive materials.[2]

Supramolecular gel synthesis encompasses a fascinating array of solvents that play a pivotal role in the creation of these intricate structures. From common solvents such as water,[10] acetonitrile,[11] ethanol,[12] and methanol[13] to more specialized ones such as dichloromethane,[14] deuterated dichloromethane,[15] 1,2-dichlorobenzene,[16] acetone,[17] carbon tetrachloride,[18] DMF,[19] tetrahydrofuran,[20] dimethyl sulfoxide,[21] and toluene,[22] each solvent brings its unique properties to the process. By interacting with organic and/or inorganic gelators, these solvents facilitate the formation of three-dimensional networks that define the gel's characteristics. The choice of solvent not only influences the gel's physical properties but also contributes to its potential applications, making solvent selection a critical aspect of designing supramolecular gels with tailored properties.

The literature is replete with a plethora of low molecular weight gelators, encompassing alkenes,[23] amides,[24] modified amino acids,[25] urea,[26] peptides,[27] sugars,[28] dendrimers,[29] and more. These gelators exhibit remarkable gelation properties in the presence of diverse solvent molecules. The formation of supramolecular gels arises from captivating non-covalent interactions, including hydrogen bonds,[30] electrostatic interactions,[31] hydrophobic[32] and hydrophilic forces,[33] van der Waals forces,[30] and aryl-system-based interactions.[34] The realm of supramolecular gels has emerged as a pivotal domain within materials science, finding applications across academia and industry alike. Notably, these gels are integral to catalysis,[10a,b] lithography,[35] opto-electronic and electrochemical devices,[36,37] chemo-sensors,[38] cell culture,[39] drug delivery,[40] tissue engineering,[41] and semiconductors.[19]

Metallogels represent a significant subset of supramolecular gels, resulting from the synergistic interaction between metal ions and appropriate low molecular weight gelators (LMWGs). This collaboration gives rise to intricate 3D supramolecular soft gel structures characterized by intriguing and unconventional properties. Within metallogels, the incorporation of metal ions introduces a range of noteworthy functionalities, including redox activity,[42] magnetic behavior,[43] conductivity,[44] actuation,[45] catalytic activity,[46] and optical attributes.[47] Transition metal-based supramolecular metallogel systems have garnered attention for their practicality and accessibility as smart functional materials. Different metal ions such as cobalt(II),[48] nickel(II),[49] copper(II),[19b] cadmium(II),[19a] iron(II/I II),[50] zinc(II),[19c,d] and manganese(II)[1] have emerged as noteworthy contributors to this field, offering diverse applications across scientific domains. Zinc(II) metallogels are a type of soft material formed by the self-assembly of Zn(II)-metal ions and organic ligands into a three-dimensional network structure. These materials have garnered interest due to their potential applications in various fields. Notably, Zn(II)-ion-based metallogels have proven particularly impactful, finding utility in drug delivery,[51] anti-pathogenic activity,[52] fluorescence sensors,[38b] electrocatalysis,[53] semiconducting devices,[19c,d] *etc.*

Schottky diodes based on metallogels hold significant importance across various applications, owing to several key advantages. Firstly, metallogels provide a platform for fine-tuning electronic properties through the selection of specific metals and ligands during synthesis. This tunability grants precise control over the energy band structure and electronic behavior of Schottky diodes, facilitating the customization of device characteristics to meet specific requirements. Secondly, metallogels exhibit exceptional stability, ensuring prolonged performance and reliability of Schottky diodes. Their robust structure and resistance to degradation make them well-suited for deployment under diverse environmental conditions and in diverse applications. Thirdly, metallogels can be manufactured using a variety of techniques, including solution processing, self-assembly, and templating methods. This versatility in fabrication allows compatibility with different substrates and facilitates scalable production, streamlining the incorporation of metallogel-based Schottky diodes into various electronic devices. Furthermore, metallogels readily integrate with other electronic components, such as transistors and sensors, due to their compatibility with diverse materials and fabrication techniques. This seamless integration paves the way for the development of multifunctional devices and systems, enhancing overall performance and functionality. In summary, Schottky diodes based on metallogels offer a unique combination of advantages, including adjustable electronic properties, stability, versatile fabrication methods, tailored surface characteristics, and compatibility with other electronic components. These attributes render them indispensable across a wide spectrum of electronic applications where precise control of device properties and dependable performance are paramount.

Broadly, the role of dicarboxylic acids as low molecular weight gelators in metallogel-research is highly precious.[19] Recent research by Dhibar *et al.* has demonstrated the utilization of metallogels in developing metal–semiconductor (MS) junction devices for applications such as Schottky barrier diodes. Dhibar and colleagues have undertaken noteworthy research in the realm of metallogel-based Schottky diode applications. Their innovative investigations center on leveraging metallogels for the development of Schottky barrier diodes, which hold crucial significance in electronic device engineering. The team's pioneering work highlights the potential of metallogels to serve as a critical component in the construction of metal–semiconductor (MS) junction devices with Schottky barrier properties. These diodes exhibit intriguing electronic behavior and have implications across various fields, including electronics, photonics, and optoelectronics. Dhibar *et al.* expanded the horizons of materials research within the realm of

Open Access Article. Published on 26 October 2023. Downloaded on 2/20/2026 1:25:55 PM.
This article is licensed under a Creative Commons Attribution-NonCommercial 3.0 Unported Licence.

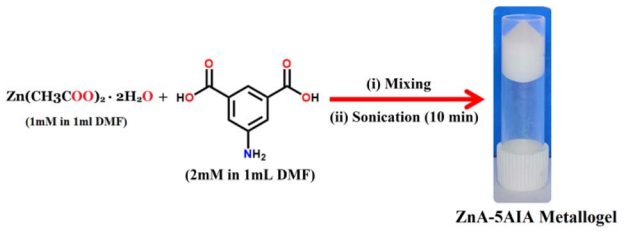

Scheme 1 The gelation process involves the following synthetic procedure, leading to the formation of a Zn(II)-metallogel (ZnA-5AIA). Subsequently, a photographic image of the obtained ZnA-5AIA metallogel is presented.

Schottky diode applications by employing a straightforward metallogel synthesis approach that does not require the use of harsh reaction conditions. This showcases the remarkable versatility and adaptability of metallogel systems in the development of advanced devices with enhanced functionality. Their findings open up exciting possibilities for the integration of novel materials in semiconductor device engineering, promising advancements in electronic and optoelectronic technologies. In line with the prevailing trajectory, we present a comprehensive synthesis procedure for a room-temperature-stable metallogel featuring Zinc(II)-ions and 5-aminoisophthalic acid as a low molecular weight gelator (LMWG) within a DMF medium (Scheme 1). This innovative approach serves as a foundation for generating tunable and enduring electronic devices. The Zn(II)-metallogel, denoted as ZnA-5AIA, exhibited robustness against gravitational forces, as demonstrated by the inversion vial test (Scheme 1). Our study encompasses the assessment of mechanical attributes and the elucidation of morphological profiles. With the ultimate goal of realizing metallogel-mediated metal–semiconductor (MS) junction devices, we accomplished the fabrication of a Schottky barrier diode (SD).

2. Experimental

2.1. Materials

Zinc(II) acetate dihydrate (98%) and 5-aminoisophthalic acid (94%) were purchased from the Sigma-Aldrich chemical company and used as received. Dry solvents (*i.e.* *N*,*N*-dimethyl formamide (DMF) were used for the entire work.

2.2. Apparatus and measurements

UV-vis absorption spectral data were collected using a SHIMADZU UV-3101PC spectrophotometer.

Rheology experiments were conducted using an Anton Paar 100 rheometer with a cone and plate geometry (CP 25-2), maintaining a fixed gap distance of 0.05 mm between the cone and plate. Gel samples were placed on the rheometer plate for mechanical measurements. An oscillatory strain amplitude sweep was performed at a constant 1 Hz oscillation frequency and in a strain range of 0.001–10% at 20 °C.

Microstructural analysis was carried out using a Carl Zeiss SUPRA 55VP FESEM instrument, while EDX elemental mapping studies were conducted using the ZEISS EVO 18 apparatus.

Infrared (IR) studies utilized a Shimadzu FTIR-8400S FTIR spectrometer.

The gel's melting point (T_{gel}) was determined using a digital gel melting point measurement apparatus (Aplab MPA-01).

For electrical characterization, the current density–voltage (*J*–*V*) characteristics were assessed using a Keithley 2635B source meter through a two-probe technique within a bias voltage range of ±1 V. The Schottky diode's conductivity was measured under dark conditions. All experiments were performed at room temperature.

2.3. Synthetic procedure of the Zn(II)-metallogel (ZnA-5AIA)

A white colour stable Zn(II)-metallogel (ZnA-5AIA) was synthesized by one shot mixing of 1 mL DMF solution of Zinc(II) acetate dihydrate (0.219 g, 1 mmol) and 1 mL DMF solution of 5-aminoisophthalic acid (0.362 g, 2 mmol) followed by continuous sonication of the mixture for 10 minutes at room temperature (Scheme 1). The inversion vial of the ZnA-5AIA metallogel proves its stability against the gravitational force (Scheme 1). The minimum critical gelation concentration (MGC) of the ZnA-5AIA metallogel was recorded at ~581 mg mL^{-1}. The concentrations of $Zn(CH_3COO)_2 \cdot 2H_2O$ and 5-aminoisophthalic acid were varied in a certain range (*i.e.* 30–581 mg mL^{-1}) to evaluate the MGC of ZnA-5AIA metallogel. Here, the ratio of the ZnA-5AIA metallogel forming components was maintained as $[Zn(CH_3COO)_2 \cdot 2H_2O]$: [5-aminoisophthalic acid] = 1 : 2, (w/w). The white colour stable ZnA-5AIA metallogel was obtained at a 581 mg mL^{-1} concentration of Zn(II)-acetate salt and 5-aminoisophthalic acid in DMF solvent. The gel melting temperature (T_{gel}) of the Zn@5AIA metallogel was recorded as 120 °C ± 2 °C *via* a digital melting-point measuring apparatus.

3. Results and discussion

3.1. Rheological analysis

The mechanical characteristics of the ZnA-5AIA metallogel were meticulously evaluated using a rheometer instrument, encompassing both angular frequency and strain-sweep measurements. The evident dominance of storage modulus (G') over loss modulus (G'') serves as confirmation of the gel-like nature of the examined sample. Particularly intriguing is the outcome of the rheological analysis conducted at a specific concentration of $Zn(CH_3COO)_2 \cdot 2H_2O$ and 5-aminoisophthalic acid (MGC = 581 mg mL^{-1}). In this investigation, the superiority of G' over G'' for the ZnA-5AIA metallogel, as evidenced in Fig. 1, substantiates its gel-like consistency, exhibiting a behavior akin to that of semi-solid materials.

Impressively, the average storage modulus of the ZnA-5AIA metallogel, measuring $G' > 10^5$ Pa, distinctly outperforms the loss modulus (G''), a testament to the material's notable mechanical resilience (Fig. 1). Complementing these findings, as shown in Fig. 2, a strain-sweep experiment was conducted on the ZnA-5AIA metallogel, with a constant angular frequency of 6.283 rad s^{-1}. The outcomes unveil a pivotal observation, a critical strain of 0.45%, marking the initiation of gel

© 2023 The Author(s). Published by the Royal Society of Chemistry

Open Access Article. Published on 26 October 2023. Downloaded on 2/20/2026 1:25:55 PM.
This article is licensed under a Creative Commons Attribution-NonCommercial 3.0 Unported Licence.

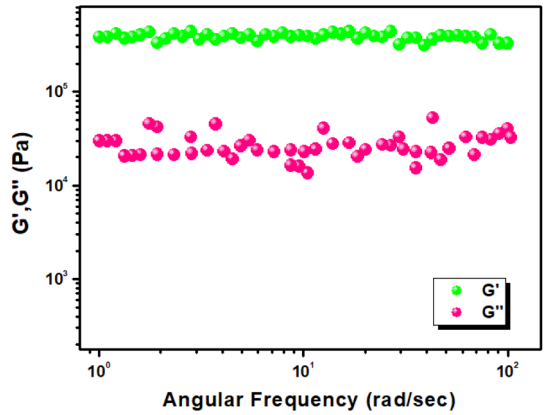

Fig. 1 The relationship between angular frequency measurements and the storage modulus (G') and loss modulus (G'') of the ZnA-5AIA metallogel.

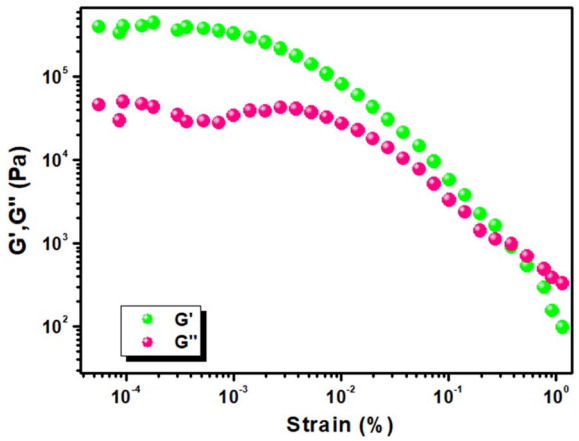

Fig. 2 Strain-sweep experiments conducted on the ZnA-5AIA metallogel, maintaining a consistent frequency of 6.283 rad s^{-1}.

breakdown. This crossover point becomes evident as G' and G'' intersect, an indicator of the transition from the gel to sol transition (Fig. 2).[54]

These combined results contribute to a comprehensive understanding of the mechanical behavior of the ZnA-5AIA metallogel, shedding light on its gel-like attributes, robustness, and the critical point at which its structural integrity shifts under strain.

3.2. Morphological analysis

The FESEM morphological analysis of the ZnA-5AIA metallogel reveals a distinctive hierarchical network characterized by flake-like patterns (as depicted in Fig. 3a–d).

These structural arrangements within the ZnA-5AIA metallogel emerged through the synergistic combination of $Zn(OAc)_2 \cdot 2H_2O$ and 5-aminoisophthalic acid in DMF solvent, facilitated by continuous sonication. The resulting FESEM image showcases the horizontally elongated flake-like morphology, underscoring the intricate nature of the formed networks. The elemental mapping further corroborates the

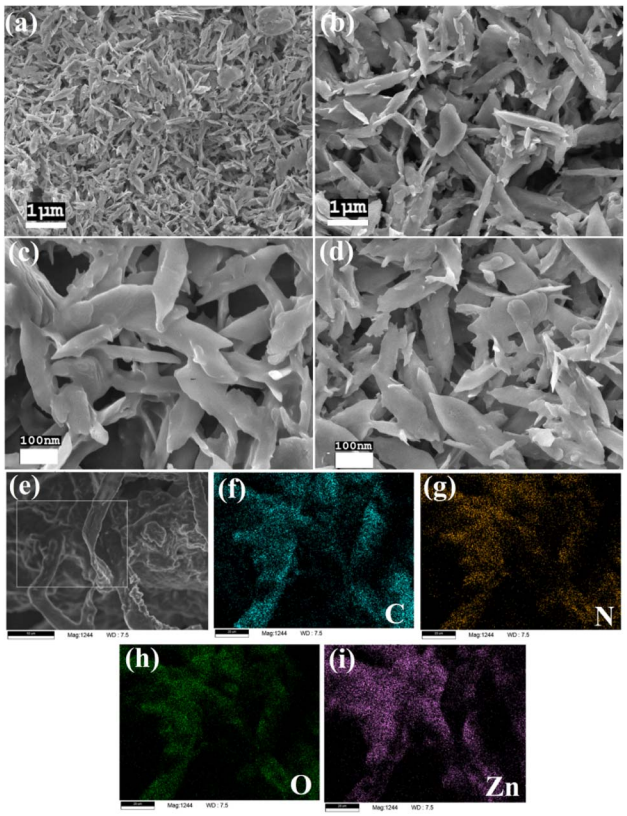

Fig. 3 The FESEM microstructural pattern of the ZnA-5AIA metallogel is displayed in (a–d), while the chemical compositions determined through elemental mapping are presented in (e–i).

composition of the network, confirming the presence of carbon (C), nitrogen (N), oxygen (O), and zinc (Zn) elements arising from $Zn(OAc)_2 \cdot 2H_2O$, 5-aminoisophthalic acid, and DMF molecules. This collective elemental makeup is responsible for the creation and organization of the distinct ZnA-5AIA metallogel network structures, as evidenced by the elemental mapping (Fig. 3e–i). Please see Fig. S1 in the ESI† for EDX spectrum analysis of ZnA-5AIA metallogel. The FESEM analysis thus provides valuable insights into the microstructural intricacies and elemental composition underlying the formation of the hierarchical flake-like network in the ZnA-5AIA metallogel.

3.3. FT-IR and PXRD analysis of ZnA-5AIA metallogel

As shown in Fig. 4, the FTIR spectrum examines the emission and absorption of materials in the infrared (IR) region. The distinct vibrations of functional groups serve as fingerprints that reveal their presence, and vibrational bands are assigned to verify the identity of these groups. Alterations in the local environment can affect these vibrations, leading to shifts in wavelengths, either shorter or longer. Even minor variations in the microenvironment are readily detected through spectroscopic analysis. Fig. 4 shows the FTIR spectrum of 5-aminoisophthalic acid and zinc acetate which are the constituents of the ZnA-5AIA metallogel. In xerogel form, the FT-IR spectrum of the ZnA-5AIA metallogel reveals significant peaks at 3280–3120, 2930, 1622, 1354, and 1155 cm^{-1},

Open Access Article. Published on 26 October 2023. Downloaded on 2/20/2026 1:25:55 PM.
This article is licensed under a Creative Commons Attribution-NonCommercial 3.0 Unported Licence.

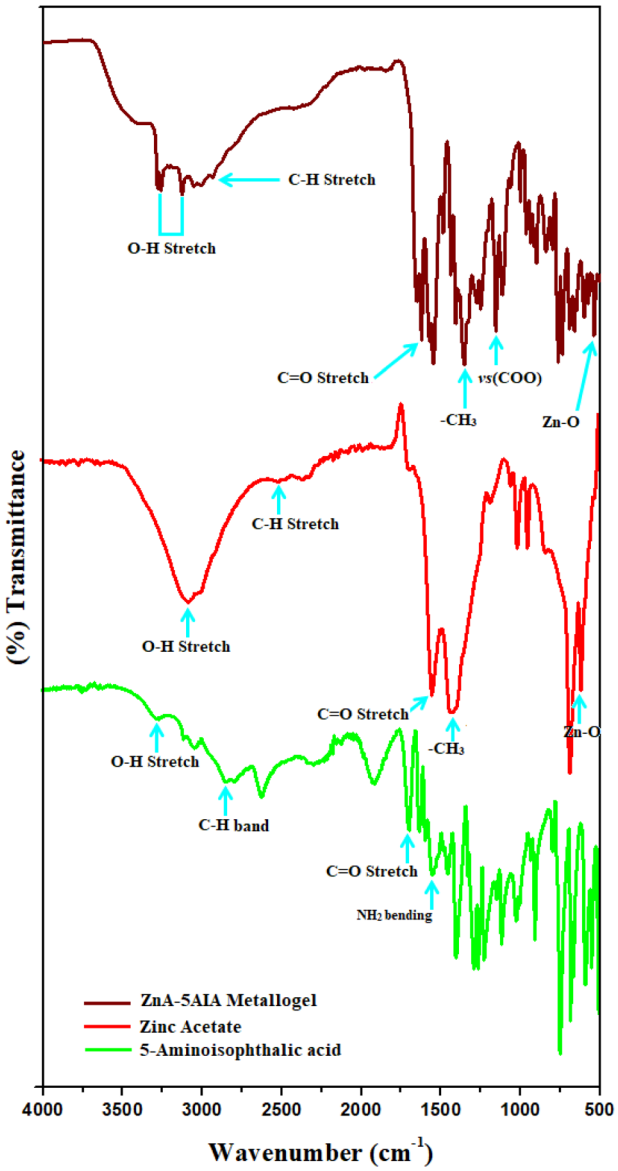

Fig. 4 FT-IR spectra of the xerogel form of the ZnA-5AIA metallogel, zinc acetate and 5-aminoisophthalic acid.

corresponding to OH stretching, –CH stretching, C=O (carboxylic) stretching, $–CH_3$, and vs(COO) vibrations, respectively. Notably, an additional peak at 538 cm^{-1} is attributed to Zn–O stretching vibrations (as shown in Fig. 4). The FT-IR data highlight the supramolecular interactions among the constituent components, delineating the intricate chemistry involved in ZnA-5AIA metallogel formation. Fig. 4 shows the FTIR spectrum of 5-aminoisophthalic acid and zinc acetate which are the constituents of the ZnA-5AIA metallogel. Vibrations of O–H stretching in the hydroxyl group are present at 3061 cm^{-1} in zinc acetate. The peak at 2489 cm^{-1} in zinc acetate represents C–H stretching. The peak at 1546 cm^{-1} in zinc acetate represents C=O stretching. The vibrations at 1429 cm^{-1} are the fingerprint vibrations of $–CH_3$. Notably, an additional peak at 617 cm^{-1} is attributed to Zn–O stretching vibrations. Compounds with acetate anions must have two vibrations in the 1350–1600 cm^{-1} range. The O–H and C=O

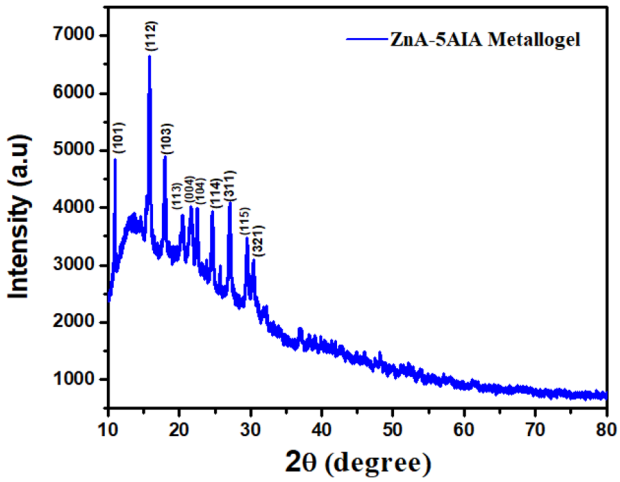

Fig. 5 Powder X-ray diffraction (PXRD) pattern of the ZnA-5AIA metallogel in xerogel.

stretching bands of the acid group appear at 3250 and 1687 cm^{-1}, respectively, while those of the NH_2 bending frequency appear at 1542 cm^{-1}. The CH band appears at 2830 cm^{-1}. The ZnA-5AIA metallogel has vibrations from both the constituents.

The ZnA-5AIA metallogel's nature was analyzed using powder X-ray diffraction (Fig. 5). The diffraction pattern exhibited ten sharp peaks at specific 2θ values 10.99°, 15.73°, 17.95°, 20.33°, 21.64°, 22.55°, 24.62°, 26.98°, 29.50°, and 30.24°, respectively. Other peaks were narrow. The sharp and narrow peaks indicate a high degree of crystallinity in the synthesized compound. Based on the XRD profiles at room temperature, the presence of zinc acetate and 5-aminoisophthalic acid was identified. Specifically, the 2θ values such as 10.99° corresponded to zinc acetate monohydrate, 15.73° corresponded to zinc acetate, 17.95° corresponded to both zinc acetate monohydrate and zinc acetate, 26.98° corresponded to 5-aminoisophthalic acid and 29.50° and 30.24° corresponded to DMF.

3.4. Fabrication of a thin film device

The Schottky device configuration employed an ITO/ZnA-5AIA/Al sandwich structure. To prepare the ITO substrate, sequential ultrasonic cleanings were carried out for 20 minutes each to perform a typical wet cleaning process using soap solution,

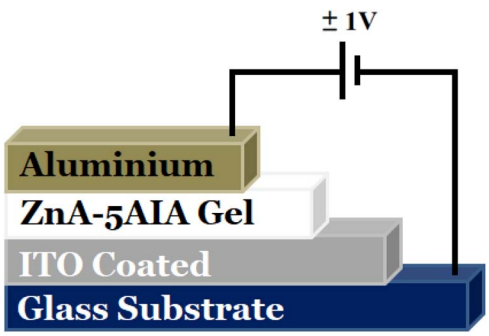

Scheme 2 Schematic representation of a metal–semiconductor (MS) junction device utilizing the ZnA-5AIA metallogel.

© 2023 The Author(s). Published by the Royal Society of Chemistry

Open Access Article. Published on 26 October 2023. Downloaded on 2/20/2026 1:25:55 PM.
This article is licensed under a Creative Commons Attribution-NonCommercial 3.0 Unported Licence.

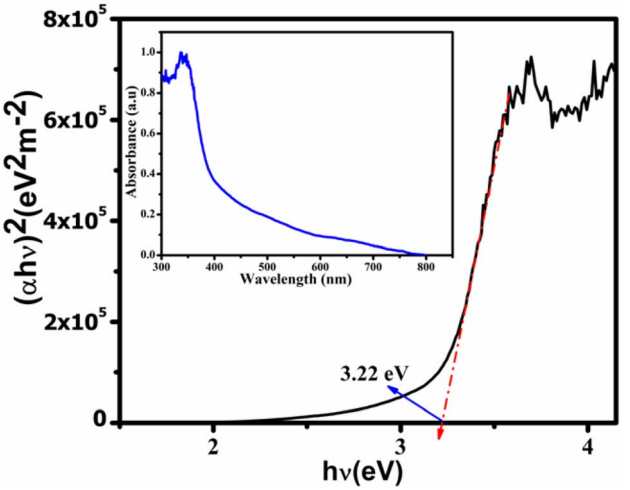

Fig. 6 $(\alpha h\gamma)^2$ *versus* $h\gamma$ curves of ZnA-5AIA, and UV-vis absorption spectra (inset) were determined with the help of Tauc's equation.

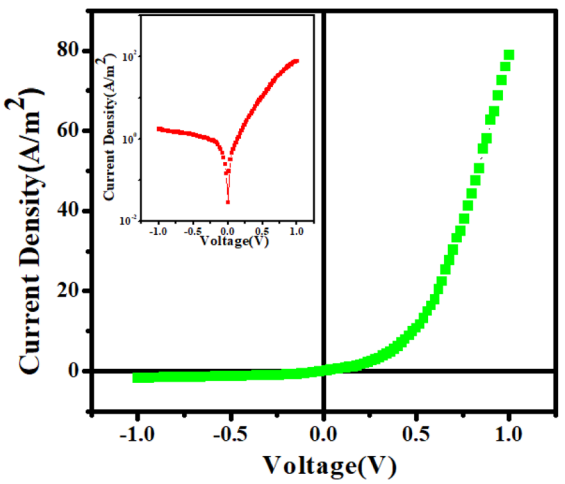

Fig. 7 Current density–voltage (*J–V*) graph of artificial gel under dark conditions. The insets show respective *J vs. V* plots (in log scale).

acetone, ethanol, and distilled water. Finally they are dried by annealing in the presence of N_2 for 15 minutes. Aluminium was selected as the contact metal to form a metal–semiconductor junction, establishing the rectifier behavior (Scheme 2).

3.5. Optical characterization

For optical band gap measurement we recorded absorption spectra of this synthesized gel in the wave length region 300 to 800 nm with a UV-Vis spectrophotometer and the recorded spectra are shown in Fig. 6 (inset). The optical band gap was determined from the analysis of the Tauc plot using the equation

$$\alpha h\nu = A(h\nu - E_g)^n$$

where α = absorption coefficient, h = Planck's constant, ν = frequency of light, A = energy dependent constant (which is taken as 1), E_g = band gap, and n = electron transition process dependent constant (for direct transition $n = 1/2$). The $(\alpha h\nu)^2$ *vs.* $h\nu$ plot is shown in Fig. 6. From Fig. 6 by extrapolation of the linear portion of the curve we can conclude that the material possesses a direct optical band gap 3.22 eV.

3.6. Electrical characterization of the device

Fig. 7 shows the current density (J) *vs.* voltage (V) graphs measured under dark conditions. We have fabricated different devices with varying film thicknesses of the ZnA-5AIA metallogel but based on the comparative study of their electrical parameters (see Table S1 in the ESI†) here we have chosen the device with film thickness about 1.0 μm for analyses. The *J–V* characteristics curve of all the fabricated devices with varying thicknesses of thin films is shown in Fig. S2 in the ESI.† The nature of the *J–V* characteristic exhibits considerable non-linearity in the scan voltage range, implying a non-ohmic conduction mechanism. This property is similar to that of the Schottky barrier diode's rectification. In the inset of Fig. 7, the log J *vs.* log V plot is shown. The rectification ratio was measured and for this compound-based diode it was found to be 45.11. The estimated conductivity for this compound-based diode at room temperature was 1.34×10^{-5} (see Table 1). This is one of the necessary and crucial characteristics of a material that can be used in photovoltaic applications.[55]

The *J–V* characteristics of the Schottky diode are further studied employing thermionic emission (TE) theory, and Cheung's method was employed to extract the important diode parameters.[56,57]

According to thermionic emission theory, the forward bias current density can be expressed as

$$J = J_0\left[\exp\left(\frac{qV}{\eta KT}\right) - 1\right] \quad (1)$$

$$J_0 = \text{saturation current density} = A^*T^2\exp\left(-\frac{q\Phi_B}{KT}\right) \quad (2)$$

where q = electronic charge, V = applied voltage, η = ideality factor, K = Boltzman's constant, T = temperature in kelvin

Table 1 Electrical parameters of the ZnA-5AIA metallogel based SD

Rectification ratio	Conductivity (S m^{-1})	Series resistance (Ω) from dV/dln*J* *vs. J* curve	Series resistance (Ω) from *H vs. J* curve	Ideality factor (η)	Barrier height φ_b (eV)
45.11	1.34×10^{-5}	0.58 K	0.53 K	4.91	0.69

Open Access Article. Published on 26 October 2023. Downloaded on 2/20/2026 1:25:55 PM.
This article is licensed under a Creative Commons Attribution-NonCommercial 3.0 Unported Licence.

scale, Φ_B = barrier potential height, and A^* = Richardson's constant and was considered as 1.2×10^6 A m^{-2} K^{-2}.

According to Cheung's model, when a series resistance is designed as a series combination of a resistor and diode, then the voltage across the diode can be substituted as the voltage drop across the series combination of the diode and resistor. Then eqn (1) can be drafted as,

$$J = J_0\left[\exp\left(\frac{q(V - IR_S)}{\eta KT}\right)\right] \quad (3)$$

where the IR_S term indicates the voltage drop across the series resistance of the semiconductor diode. Inserting the value of saturation current density into eqn (3) and differentiating with respect to ln$J$, we get,

$$\frac{dV}{d\ln J} = AJR_S + \frac{\eta KT}{q} \quad (4)$$

where R_s = series resistance, q = electronic charge, η = ideality factor, K = Boltzman's constant, and T = temperature on the Kelvin scale.

As stated in the Cheung model, the current density-reliant function $H(J)$ can be written as,

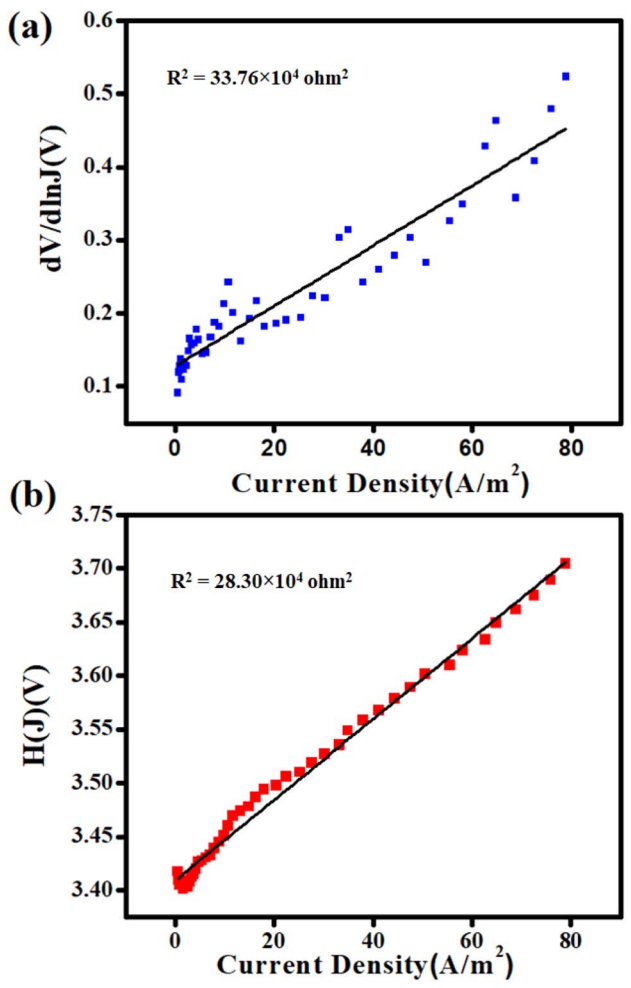

Fig. 8 (a) Under dark conditions, dV/dln$J$ *vs.* J; (b) $H(J)$ *vs.* J curves in the double y-axis.

Table 2 Comparison table of electrical parameters of the ZnA-5AIA metallogel based device with other reported results

Device based on	Rectification ratio	Conductivity (S m^{-1})	Ideality factor (η)	Barrier height (φ_B) (eV)	Series resistance R_S (Ohm)		Ref.
					dv/dln$J$ *vs.* J	$H(J)$ *vs.* J	
ZnA-5AIA	45.11	1.34×10^{-5}	4.91	0.69	0.58 K	0.53 K	This work
Zn@TA	37.06	7.77×10^{-6}	3.78	0.47	3751.26	3587.73	59
Zn-SA	20.83	6.72×10^{-6}	2.53	0.70	2890	3000	52
Zn-SB	14.63	1.18×10^{-6}	3.93	0.75	37 340	3930	60
ZnCdS	29	—	2.22	0.28	17.3 K	24.9 K	61

© 2023 The Author(s). Published by the Royal Society of Chemistry

Open Access Article. Published on 26 October 2023. Downloaded on 2/20/2026 1:25:55 PM. This article is licensed under a Creative Commons Attribution-NonCommercial 3.0 Unported Licence.

$$H(J) = V - \frac{\eta KT}{q}\ln\left(\frac{J}{A^*T^2}\right) = AJR_S + \eta\Phi_B \quad (5)$$

where Φ_B = barrier height and A^* = Richardson's constant and was considered as 1.2×10^6 A m^{-2} K^{-2}

The curve of dV/dln(J) *vs.* J in Fig. 8a is linear. The y-axis intercept of this figure yields the ideality factors (η) of the SBD. The diodes' barrier height (φ_b) is calculated from the y-axis intercept of the $H(J)$ *vs.* J linear plot shown in Fig. 8b. Table 1 shows the measured ideality factor and barrier height for the Al/ZnA-5AIA junction. The ideality factor for the compound based device deviated from unity, as can be seen.

Multiple generation recombination of charge carriers in the junction region *via* interface traps and inhomogeneous barrier height is the cause of the variation.[58] The calculated barrier height for the Al/ZnA-5AIA metallogel junction is 0.69 eV.

We have compared the electrical parameters of the current materials based SBD with other reported results and all the data are tabulated below. Table 2 shows that our synthesized material has greater electrical conductivity and higher rectification ratio and lower series resistance than other materials reported.

4. Conclusions

In summary, a pioneering approach was employed to synthesize a novel supramolecular Zn(II)-metallogel utilizing 5-aminoisophthalic acid as the gelator. The gel was swiftly formed through the immediate mixing of zinc acetate and 5-aminoisophthalic acid in DMF, followed by sonication under ambient conditions. The resultant stable ZnA-5AIA metallogel owes its structure to a medley of non-covalent interactions, facilitating its formation at room temperature. Microstructural analysis *via* FESEM unraveled the intriguing hierarchical flake-like architecture of the hydrogel. Mechanical assessments established the robustness of the ZnA-5AIA metallogel material, evidenced through rheological examinations. Notably, optical band-gap measurements indicated the semiconducting nature of the synthesized ZnA-5AIA metallogel. The fabrication of a thin film device incorporating the ZnA-5AIA metallogel as a semiconducting component alongside Au metal yielded a metal–semiconductor junction. The nonlinear charge transport observed in the *I–V* characteristic graph validated the realization of a Schottky diode. This study presents a noteworthy configuration of ITO/ZnA-5AIA metallogel/Au, underscoring its potential for future advancements in supramolecular Zn(II) metallogel-based electronic devices. The successful synthesis and characterization of the ZnA-5AIA metallogel, grounded in 5-aminoisophthalic acid and zinc(II) components, hold promise as a pioneering strategy for semiconducting device fabrication. The outcomes of this research illuminate a promising path toward the development of innovative technologies. By harnessing the distinctive properties of supramolecular metallogels, the study extends the horizon for the creation of advanced electronic devices. Ultimately, the demonstrated methodology offers an impactful contribution to the field, providing novel insights and avenues for the integration of metallogels in semiconducting device applications.

Conflicts of interest

The authors declare no competing financial interests.

Acknowledgements

S.D. expresses gratitude to the UGC, New Delhi, for the conferred Dr DS Kothari Postdoctoral Fellowship (Award letter number: No. F.4-2/2006 (BSR)/CH/19-20/0224). B. P. acknowledges the financial backing of this endeavor through DST-INSPIRE, GOI. S. B. appreciates the support from the DST Inspire Faculty Research Grant (Faculty Registration No. IFA18-CH304; DST/INSPIRE/04/2018/000329).

Notes and references

1 S. Dhibar, A. Dey, S. Majumdar, D. Ghosh, P. P. Ray and B. Dey, *ACS Appl. Electron. Mater.*, 2019, **1**, 1899–1908.
2 P. Dastidar, *Chem. Soc. Rev.*, 2008, **37**, 2699–2715.
3 A. Noro, M. Hayashia and Y. Matsushita, *Soft Matter*, 2012, **8**, 6416–6429.
4 E. Ye, P. L. Chee, A. Prasad, X. Fang, C. Owh, V. J. J. Yeo and X. J. Loh, *Mater. Today*, 2014, **17**, 194–202.
5 D. Rambabu, P. Negi, A. Dhir, A. Gupta and Pooja, *Inorg. Chem. Commun.*, 2018, **93**, 6–9.
6 S. R. Jadav, P. K. Vemula, R. Kumar, S. R. Raghavan and G. John, *Angew. Chem., Int. Ed.*, 2010, **49**, 7695–7698.
7 M. Suzuki and K. Hanabusa, *Chem. Soc. Rev.*, 2010, **39**, 455–463.
8 P. Terech and R. G. Weiss, *Chem. Rev.*, 1997, **97**, 3133–3159.
9 J. Raeburn and D. J. Adams, *Chem. Commun.*, 2015, **51**, 5170–5180.
10 (*a*) S. Dhibar, D. Ghosh, S. Majumdar and B. Dey, *ACS Omega*, 2020, **5**, 2680–2689; (*b*) S. Dhibar, A. Dey, R. Jana, A. Chatterjee, G. K. Das, P. P. Ray and B. Dey, *Dalton Trans.*, 2019, **48**, 17388–17394.
11 C. Po, Z. Ke, A. Y. Y. Tam, H. F. Chow and V. W. W. Yam, *Chem.–Euro. J.*, 2013, **19**, 15735–15744.
12 Q. Lin, Q.-P. Yang, B. Sun, Y.-P. Fu, X. Zhu, T.-B. Wei and Y.-M. Zhang, *Soft Matter*, 2014, **10**, 8427–8432.
13 (*a*) C. K. Karan and M. Bhattacharjee, *ACS Appl. Mater. Interfaces*, 2016, **8**, 5526–5535; (*b*) S. Dey, D. Datta, K. Chakraborty, S. Nandi, A. Anoop and T. Pathak, *RSC Adv.*, 2013, **3**, 9163–9166; (*c*) M.-O. M. Piepenbrock, N. Clarke and J. W. Steed, *Soft Matter*, 2010, **6**, 3541–3547.
14 (*a*) Z. Yao, Z. Wang, Y. Yu, C. Zeng and K. Cao, *Polymer*, 2017, **119**, 98–106; (*b*) P. Rajamalli, P. Malakar, S. Atta and E. Prasad, *Chem. Commun.*, 2014, **50**, 11023–11025.
15 K. Mitsumoto, J. M. Cameron, R.-J. Wei, H. Nishikawa, T. Shiga, M. Nihei, G. N. Newton and H. Oshio, *Chem.–Euro. J.*, 2017, **23**, 1502–1506.
16 X.-Q. Wang, W. Wang, G.-Q. Yin, Y.-X. Wang, C.-W. Zhang, J.-M. Shi, Y. Yu and H.-B. Yang, *Chem. Commun.*, 2015, **51**, 16813–16816.
17 B. Jiang, L.-J. Chen, G.-Q. Yin, Y.-X. Wang, W. Zheng, L. Xu and H.-B. Yang, *Chem. Commun.*, 2017, **53**, 172–175.

© 2023 The Author(s). Published by the Royal Society of Chemistry

Open Access Article. Published on 26 October 2023. Downloaded on 2/20/2026 1:25:55 PM. This article is licensed under a Creative Commons Attribution-NonCommercial 3.0 Unported Licence.

18 (*a*) F. Gou, J. Cheng, X. Zhang, G. Shen, X. Zhou and H. Xiang, *Eur. J. Inorg. Chem.*, 2016, 4862–4866; (*b*) N. Kelly, K. Gloe, T. Doert, F. Hennersdorf, A. Heine, J. Marz, U. Schwarzenbolz, J. J. Weigand and K. J. Gloe, *Organomet. Chem.*, 2016, **821**, 182–191.

19 (*a*) S. Dhibar, A. Dey, S. Majumdar, D. Ghosh, A. Mandal, P. P. Ray and B. Dey, *Dalton Trans.*, 2018, **47**, 17412–17420; (*b*) S. Dhibar, S. K. Ojha, A. Mohan, S. P. C. Prabhakaran, S. Bhattacharjee, K. Karmakar, P. Karmakar, P. Predeep, A. K. Ojha and B. Saha, *New J. Chem.*, 2022, **46**, 17189–17200; (*c*) S. Dhibar, S. Babu, A. Mohan, G. K. Chandra, S. Bhattacharjee, K. Karmakar, P. Karmakar, S. M. Rahaman, P. Predeep and B. Saha, *J. Mol. Liq.*, 2023, **375**, 121348; (*d*) K. Karmakar, A. Dey, S. Dhibar, R. Sahu, S. Bhattacharjee, P. Karmakar, P. Chatterjee, A. Mondal and B. Saha, *RSC Adv.*, 2023, **13**, 2561–2569.

20 (*a*) Z. Yao, Z. Wang, Y. Yu, C. Zeng and K. Cao, *Polymer*, 2017, **119**, 98–106; (*b*) P. Rajamalli, P. Malakar, S. Atta and E. Prasad, *Chem. Commun.*, 2014, **50**, 11023–11025.

21 (*a*) S. Ganta and D. K. Chand, *Dalton Trans.*, 2015, **44**, 15181–15188; (*b*) L. Yang, L. Luo, S. Zhang, X. Su, J. Lan, C.-T. Chen and J. You, *Chem. Commun.*, 2010, **46**, 3938–3940; (*c*) B. Xing, M.-F. Choi, Z. Zhou and B. Xu, *Langmuir*, 2002, **18**, 9654–9658; (*d*) X. Ma, S. Liu, Z. Zhang, Y. Niu and J. Wu, *Soft Matter*, 2017, **13**, 8882–8885.

22 C. A. Offiler, C. D. Jones and J. W. Steed, *Chem. Commun.*, 2017, **53**, 2024–2027.

23 S. J. Wezenberg, C. M. Croisetu, M. C. A. Stuartab and B. L. Feringa, *Chem. Sci.*, 2016, **7**, 4341–4346.

24 N. Shi, G. Yin, H. Li, M. Hana and Z. Xu, *New J. Chem.*, 2008, **32**, 2011–2015.

25 K. Hanabusa, K. Hiratsuka, M. Kimura and H. Shirai, *Chem. Mater.*, 1999, **11**, 649–655.

26 J. W. Steed, *Chem. Soc. Rev.*, 2010, **39**, 3686–3699.

27 C. Tomasini and N. Castellucci, *Chem. Soc. Rev.*, 2013, **42**, 156–172.

28 A. Prathap and K. M. Sureshan, *Langmuir*, 2019, **35**, 6005–6014.

29 D. K. Smith, *Adv. Mater.*, 2006, **18**, 2773–2778.

30 R. G. Weiss and P. Terech, *Molecular Gels: Materials with Self-Assembled Fibrillar Networks*, Springer, Dordrecht, 2005.

31 (*a*) T.-A. Asoh and A. Kikuchi, *Chem. Commun.*, 2012, **48**, 10019–10021; (*b*) X. Wang, F. Liu, X. Zheng and J. Sun, *Angew. Chem., Int. Ed.*, 2011, **50**, 11378–11381; (*c*) H. Wang, M. B. Hansen, D. W. P. M. Löwik, J. C. M. van Hest, Y. Li, J. A. Jansen and S. C. G. Leeuwenburgh, *Adv. Mater.*, 2011, **23**, H119–H124.

32 (*a*) A. Y.-Y. Tam and V. W.-W. Yam, *Chem. Soc. Rev.*, 2013, **42**, 1540–1567; (*b*) C. Tomasini and N. Castellucci, *Chem. Soc. Rev.*, 2013, **42**, 156–172; (*c*) L. Meazza, J. A. Foster, K. Fucke, P. Metrangolo, G. Resnati and J. W. Steed, *Nat. Chem.*, 2013, **5**, 42–47.

33 (*a*) M. Shirakawa, N. Fujita and S. Shinkai, *J. Am. Chem. Soc.*, 2003, **125**, 9902–9903; (*b*) J. R. Moffat, G. J. Seeley, J. T. Carter, A. Burgess and D. K. Smith, *Chem. Commun.*, 2008, 4601–4603.

34 (*a*) Y. Xu, Q. Wu, Y. Sun, H. Bai and G. Shi, *ACS Nano*, 2010, **4**, 7358–7362; (*b*) S. Burattini, B. W. Greenland, D. H. Merino, W. Weng, J. Seppala, H. M. Colquhoun, W. Hayes, M. E. Mackay, I. W. HamLey and S. J. Rowan, *J. Am. Chem. Soc.*, 2010, **132**, 12051–12058.

35 J. Kim, J. A. Hanna, M. Byun, C. D. Santangelo and R. C. Hayward, *Science*, 2012, **335**, 1201–1205.

36 A. R. Hirst, B. Escuder, J. F. Miravet and D. K. Smith, *Angew. Chem., Int. Ed.*, 2008, **47**, 8002–8018.

37 X. Cheng, J. Pan, Y. Zhao, M. Liao and H. Peng, *Adv. Energy Mater.*, 2018, **8**, 1702184.

38 (*a*) S. Sarkar, S. Dutta, S. Chakrabarti, P. Bairi and T. Pal, *ACS Appl. Mater. Interfaces*, 2014, **6**, 6308–6316; (*b*) Q. Lin, T.-T. Lu, X. Zhu, B. Sun, Q.-P. Yang, T.-B. Wei and Y.-M. Zhang, *Chem. Commun.*, 2015, **51**, 1635–1638.

39 W. Wang, H. Wang, C. Ren, J. Wang, M. Tan, J. Shen, Z. Yang, P. G. Wang and L. Wang, *Carbohydr. Res.*, 2011, **346**, 1013–1017.

40 Md. R. Saboktakin and R. M. Tabatabaei, *Int. J. Biol. Macromol.*, 2015, **75**, 426–436.

41 Y. Zhao, S. Song, X. Ren, J. Zhang, Q. Lin and Y. Zhao, *Chem. Rev.*, 2022, **122**, 5604–5640.

42 W.-L. Guan, K. M. Adam, M. Qiu, Y.-M. Zhang, H. Yao, T.-B. Wei and Q. Lin, *Supramol. Chem.*, 2020, **32**, 578–596.

43 W. H. Binder, L. Petraru, T. Roth, P. W. Groh, V. Pálfi, S. Keki and B. Ivan, *Adv. Funct. Mater.*, 2007, **17**, 1317–1326.

44 A. Khan, R. R. Kisannagar, C. Gouda, D. Gupta and H.-C. Lin, *J. Mater. Chem. A*, 2020, **8**, 19954–19964.

45 B. Xue, M. Qin, T. Wang, J. Wu, D. Luo, Q. Jiang, Y. Li, Y. Cao and W. Wang, *Adv. Funct. Mater.*, 2016, **26**, 9053–9062.

46 B. Zhang and J. N. H. Reek, *Chem.–Asian J.*, 2021, **16**, 3851–3863.

47 S. Biswas, U. Chatterjee, S. Sarkar, F. Khan, D. Bera, M. Mukhopadhyay, S. Goswami, S. Chakrabarti and S. Das, *Colloids Surf., B*, 2020, **188**, 110803.

48 (*a*) N. Kelly, K. Gloe, T. Doert, F. Hennersdorf, A. Heine, J. Maerz, U. Schwarzenbolz, J. J. Weigand and K. Gloe, *J. Organomet. Chem.*, 2016, **821**, 182–191; (*b*) L. Yan, C. Liu, L. Shen, J. Li, X. Liu, M. Lv, C. Su and Z. Ye, *Chem. Lett.*, 2018, **47**, 640–642; (*c*) J. H. Lee, Y. E. Baek, K. Y. Kim, H. Choi and J. H. Jung, *Supramol. Chem.*, 2016, **28**, 870–873; (*d*) S. Dhibar, S. Babu, K. Karmakar, A. Mohan, S. Bhattacharjee, S. M. Rahaman, G. C. Nayak, R. Saha, P. Predeep and B. Saha, *Chem. Phys. Lett.*, 2023, 140777.

49 B. Pal, S. Dhibar, R. Mukherjee, S. Bhattacharjee, P. P. Ray and B. Saha, *Mater. Adv.*, 2023, **4**, 3628–3635.

50 (*a*) J. Chen, T. Wang and M. Liu, *Inorg. Chem. Front.*, 2016, **3**, 1559–1565; (*b*) J.-L. Zhong, X.-J. Jia, H.-J. Liu, X.-Z. Luo, S.-G. Hong, N. Zhang and J.-B. Huang, *Soft matter*, 2016, **12**, 191–199; (*c*) L. Arnedo-Sánchez, Nonappa, S. Bhowmik, S. Hietala, R. Puttreddy, M. Lahtinen and L. D. C. K. Rissanen, *Dalton Trans.*, 2017, **46**, 7309–7316.

51 K. Sarkar and P. Dastidar, *Chem.–Asian J.*, 2019, **14**, 194–204.

52 G. Lepcha, S. Majumdar, B. Pal, K. T. Ahmed, I. Pal, B. Satpati, S. R. Biswas, P. P. Ray and B. Dey, *Langmuir*, 2023, **39**, 7469–7483.

 © 2023 The Author(s). Published by the Royal Society of Chemistry

Open Access Article. Published on 26 October 2023. Downloaded on 2/20/2026 1:25:55 PM.
This article is licensed under a Creative Commons Attribution-NonCommercial 3.0 Unported Licence.

53 T. Zhu, Q. Feng, S. Liu and C. Zhang, *Compos. Commun.*, 2020, **20**, 100376.
54 (*a*) N. Kuroda, Y. Tounoue, K. Noguchi, Y. Shimasaki, H. Inokawa, M. Takano, S. Shinkai and S. Tamaru, *Polym. J.*, 2020, **52**, 939–946; (*b*) R. D. Mukhopadhyay, G. Das and A. Ajayaghosh, *Nat. Commun.*, 2018, **9**, 1987–1996.
55 A. Wibowo, M. A. Marsudi, M. I. Amal, M. B. Ananda, R. Stephanie, H. Ardy and L. J. Diguna, *RSC Adv.*, 2020, **10**, 42838–42859.
56 B. Pal, P. Das, J. Datta, U. Gangopadhyay and P. P. Ray, *Mater. Sci. Semicond. Process.*, 2023, **162**, 107535.
57 S. Cheung and N. Cheung, *Appl. Phys. Lett.*, 1986, **49**, 85–87.
58 P. Das, B. Pal, J. Datta, M. Das, S. Sil and P. P. Ray, *J. Phys. Chem. Solids*, 2021, **148**, 109706.
59 S. Majumdar, A. Dey, R. Sahu, G. Lepcha, A. Dey, P. P. Ray and B. Dey, *Mater. Res. Bull.*, 2023, **157**, 112003.
60 G. Lepcha, B. Pal, S. Majumdar, K. T. Ahmed, I. Pal, S. R. Biswas, P. P. Ray and B. Dey, *Mater. Adv.*, 2023, **4**, 2595–2603.
61 M. Das, J. Datta, R. Jana, S. Sil, S. Halder and P. P. Ray, *New J. Chem.*, 2017, **41**, 5476–5486.

© 2023 The Author(s). Published by the Royal Society of Chemistry